

Geophysical Research Letters

RESEARCH LETTER

10.1029/2019GL083465

Key Points:

- A seismic network-based method for the automatic 3-D location of volcanic tremors is developed
- The migration of deep volcanic tremor sources to the surface is tracked in time beneath Klyuchevskoy volcano
- The developed location method is fully automatic and can be updated continuously with new data

Supporting Information:

- Supporting Information S1

Correspondence to:

J. Soubestre,
jean.soubestre@gmail.com

Citation:

Soubestre, J., Seydoux, L., Shapiro, N. M., de Rosny, J., Droznin, D. V., Droznina, S. Y., et al. (2019). Depth migration of seismovolcanic tremor sources below the Klyuchevskoy volcanic group (Kamchatka) determined from a network-based analysis. *Geophysical Research Letters*, 46, 8018–8030. <https://doi.org/10.1029/2019GL083465>

Received 25 APR 2019

Accepted 8 JUL 2019

Accepted article online 16 JUL 2019

Published online 26 JUL 2019

Depth Migration of Seismovolcanic Tremor Sources Below the Klyuchevskoy Volcanic Group (Kamchatka) Determined From a Network-Based Analysis

J. Soubestre¹, L. Seydoux², N. M. Shapiro^{3,4}, J. de Rosny⁵, D. V. Droznin⁶, S. Ya. Droznina⁶, S. L. Senyukov⁶, and E. I. Gordeev^{6,7}

¹Instituto Volcanológico de Canarias (INVOLCAN), INtech La Laguna, Tenerife, Spain, ²Institut des Sciences de la Terre (ISTERRE), Université Grenoble-Alpes UMR CNRS 5375, Grenoble, France, ³Institut de Physique du Globe de Paris, UMR CNRS 7154, Paris, France, ⁴Schmidt Institute of Physics of the Earth, Russian Academy of Sciences, Moscow, Russia, ⁵Institut Langevin, CNRS PSL Research University, Paris, France, ⁶Kamchatka Branch of the Geophysical Survey, Russian Academy of Sciences, Petropavlovsk-Kamchatsky, Russia, ⁷Institute of Volcanology and Seismology, FEB RAS, Petropavlovsk-Kamchatsky, Russia

Abstract We present a method for automatic location of dominant sources of seismovolcanic tremor in 3-D, based on the spatial coherence of the continuously recorded wavefield at a seismic network. We analyze 4.5 years of records from the seismic network at the Klyuchevskoy volcanic group in Kamchatka, Russia, when four volcanoes experienced tremor episodes. After enhancing the tremor signal with spectral whitening, we compute the daily cross-correlation functions related to the dominant tremor sources from the first eigenvector of the spectral covariance matrix and infer their daily positions in 3-D. We apply our technique to the tremors beneath Shiveluch, Klyuchevskoy, Tolbachik, and Kizimen volcanoes and observe the yearlong preeruptive volcanic tremor beneath Klyuchevskoy from deep to shallow parts of the plumbing system. This observation of deep volcanic tremor sources demonstrates that the cross-correlation-based method is a very powerful tool for volcano monitoring.

Plain Language Summary Volcanic tremors are the seismic signature of magmatic and hydrothermal fluids passing through volcanic conduits. Locating them in 3-D is of real interest because it could allow us to monitor in more detail movements of magma inside volcanic edifices and, in some cases, to forecast eruptive episodes. The location of tremor in 3-D nevertheless remains challenging because signals generated by tremors do not present any clear onset that could be used for picking arrival times and for determining source location. We design a method based on cross correlations that recovers the differential travel times between receivers of a seismic network from the analysis of the statistically dominating waves in the wavefield. We present an application of the proposed method to volcanoes in Kamchatka, Russia, and show that we can track the preeruptive tremor episode in depth before the main eruption of the Klyuchevskoy volcano.

1. Introduction

The long-period volcanic seismicity, composed of long-period events and volcanic tremors, is mainly thought to be related to processes induced by fluid movements within magmatic or hydrothermal volcanic systems (Chouet, 1996; Iverson et al., 2006). As it constitutes an important attribute of volcanic unrest, its detection and characterization is a key aspect of volcano monitoring and eruption forecasting (Chouet & Matoza, 2013; McNutt, 1992; Sparks et al., 2012). Long-period earthquakes and volcanic tremors derive from similar processes, but they differ in nature. Long-period earthquakes are discrete emergent signals of high-frequency onset followed by a low-frequency harmonic waveform of typical frequency range 0.5–5 Hz (Chouet, 1996), that can sometimes become very frequent in episodes called “drumbeats.” Volcanic tremors are highly irregular continuous signals that can last from a few minutes to several months, of which the spectral content can be harmonic, monochromatic, banded, spasmodic, etc. (Konstantinou & Schlindwein, 2003). However, both phenomena are believed to be generated by similar mechanisms such as magma moving through nar-

row cracks, fragmentation and pulsation of pressurized fluids within the volcano, or escape of pressurized steam and gases from fumaroles (Chouet & Matoza, 2013).

Long-period earthquakes are observed in both shallow parts of volcanoes (e.g., Chouet, 1996; Ciaramella et al., 2011; Firstov & Shakirova, 2014; Frank et al., 2018; Jolly et al., 2017; Shapiro et al., 2017; Woods et al., 2018,) and deep parts (e.g., Frank et al., 2018; Han et al., 2018; Hasegawa et al., 1991; Hotovec-Ellis et al., 2018; Pitt & Hill, 1994; Shapiro et al., 2017; Ukawa & Ohtake, 1987; White, 1996; White et al., 1992), whereas most of the reported volcanic tremor sources are superficial (< 5 km). Indeed, except the deep volcanic tremors (30–60 km) observed at Kilauea volcano between 1962 and 1983 (Aki & Koyanagi, 1981; Shaw & Chouet, 1991), the majority of volcanic tremor studies deal with superficial sources. Thus, shallow volcanic tremor sources are reported on eruptive craters and conduits (e.g., Almendros et al., 2014; Battaglia et al., 2005; Di Grazia et al., 2006; Goldstein & Chouet, 1994; Ichimura et al., 2018; Métaxian et al., 2002; Moschella et al., 2018; Ogiso et al., 2015), building cones (Haney, 2010), gas slug bursts at surface vents (e.g., Barriere et al., 2017; Chouet et al., 1997; Eibl, Bean, Jónsdóttir, 2017; Fee et al., 2010; Patrick et al., 2011; Ripepe et al., 2001; Yukutake et al., 2017), lava lakes (e.g., Barriere et al., 2017; Donaldson et al., 2017; Métaxian et al., 1997), lava flows (Caudron et al., 2015), shallow dikes (e.g., Eibl, Bean, Vogfjörð, et al. 2017; Eibl, Bean, Jónsdóttir, 2017; Woods et al., 2018), magma-water aquifer interfaces (Almendros et al., 1997), etc.

Methods currently used for volcanic tremor source location can be divided into the following categories: small-aperture array methods (e.g., Almendros et al., 1997; Almendros et al., 2007; Almendros et al., 2014; Chouet et al., 1997; Eibl, Bean, Vogfjörð, et al. 2017; Eibl, Bean, Jónsdóttir, 2017; Goldstein & Chouet, 1994; Haney, 2010; Métaxian et al., 2002), network-based amplitude decay methods (e.g., Aki & Koyanagi, 1981; Battaglia et al., 2005; Di Grazia et al., 2006; Ichimura et al., 2018; Moschella et al., 2018; Ogiso et al., 2015; Ripepe et al., 2001; Taisne et al., 2011), and network-based interstations cross-correlations methods (e.g., Ballmer et al., 2013; Barriere et al., 2017; Donaldson et al., 2017; Droznin et al., 2015; Li et al., 2016, 2017; Yukutake et al., 2017; Woods et al., 2018). It is interesting to mention that network-migration-based methods have been also used to locate tectonic tremor and low-frequency earthquakes (e.g., Frank & Shapiro, 2014; Kao & Shan, 2004). Dense small-aperture arrays are not always available because of their cost and their temporal nature, but large-scale seismic networks are nowadays permanently deployed in many places. Because of assumptions about geometrical spreading and attenuation, network-based amplitude decay methods are adapted to locate volcanic tremor sources relatively close to the used network, that is, sources that are not so far or not so deep. On the other hand, interstations cross-correlations methods can observe tremors at larger scales (Ballmer et al., 2013) and might be able to locate deeper sources. Previous volcanic tremor location studies based on cross correlations have located shallow tremor sources at Kilauea (Ballmer et al., 2013; Donaldson et al., 2017), Katla (Li et al., 2016, 2017), Nyiragongo and Nyamulagira (Barriere et al., 2017), Hakone (Yukutake et al., 2017), and Bardarbunga (Woods et al., 2018) volcanoes.

To our knowledge, no deep volcanic tremor source has been located with this method so far. This is certainly due to the fact that a surface wave propagation is often assumed for the analysis, inherently implying the source to be located in the shallow part. The automatic cross-correlations-based location method proposed in our article is a 3-D approach based on the assumption of dominant *S* wave emission from tremor sources and associated *S* wave structures, enabling to look for both shallow and deep tremors. By using the daily first eigenvector of the network covariance matrix, we are able to track the temporal evolution on a daily time scale of the 3-D location of the daily dominating volcanic tremor sources.

We apply the developed method to data continuously recorded by the permanent monitoring network of the Klyuchevskoy group of volcanoes (Kamchatka, Russia; see Figure 1) during a 4.5-year-long time period between January 2009 and June 2013. During this period of time, Klyuchevskoy, Tolbachik, Kizimen, and Shiveluch volcanoes experienced episodes of volcanic tremor (Droznin et al., 2015) and abundant amount of long-period earthquakes (Shapiro et al., 2017). The two most important tremors led to a summit eruption at the end of 2010 at Klyuchevskoy (e.g., Senyukov, 2013) and a fissure eruption beginning at the end of 2012 at Tolbachik (e.g., Gordeev et al., 2013). Short explosive eruptions also occurred at Bezymianny. The seismic monitoring network and volcanic tremors acting in the studied volcanic group are described in section 2. Section 3 details the method developed to automatically locate tremor sources in 3-D. The temporal evolution of those 3-D locations is described and discussed in sections 3.3 and 4.

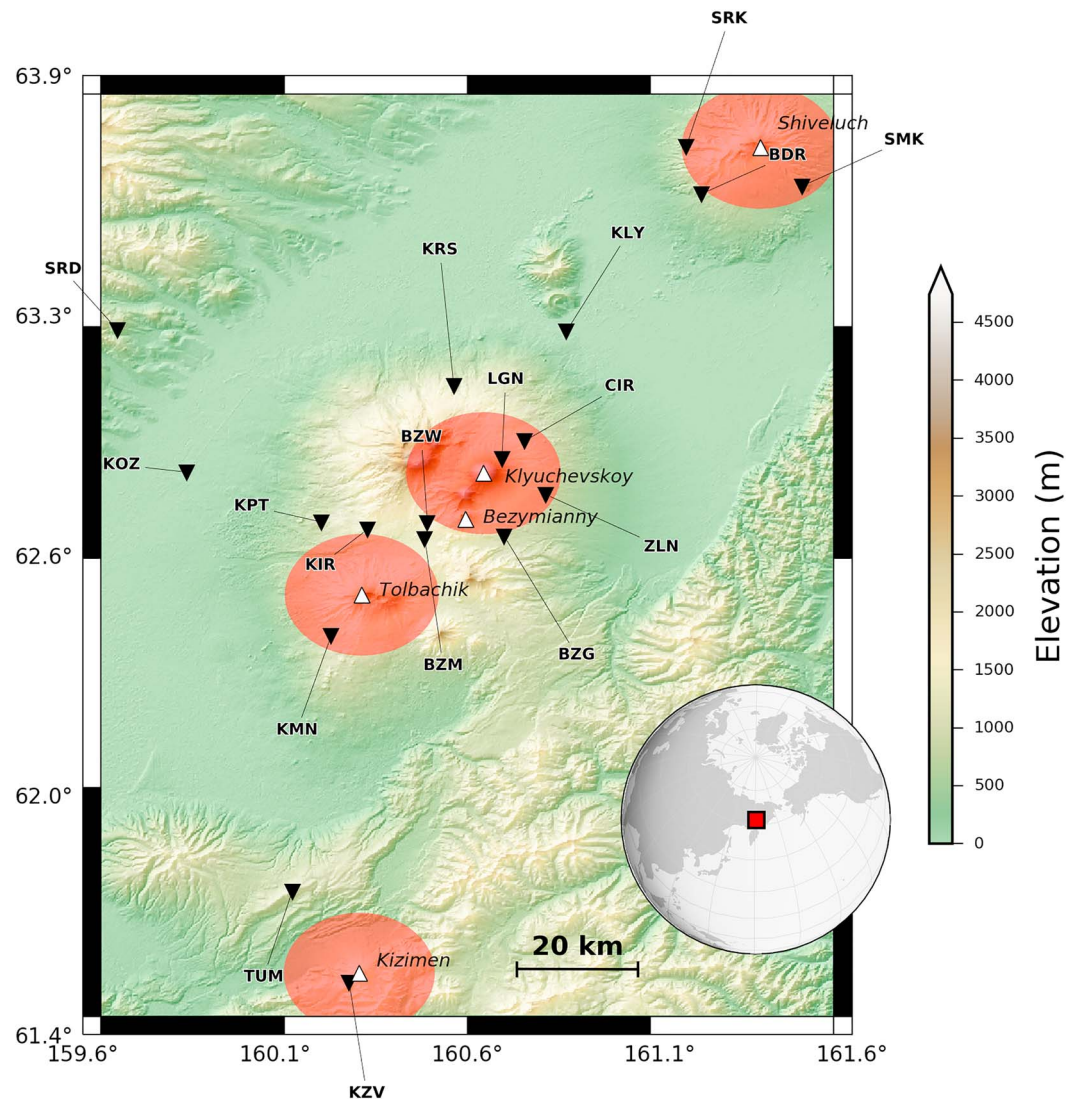


Figure 1. Seismic network (stations: black inverted triangles) monitoring the Klyuchevskoy volcanic group and surrounding volcanoes (white triangles). The Russian Kamchatka peninsula is located by a red square on the Earth globe. The 25-km radius circular zones used for the analysis of the vertical migration of volcanic tremor sources with time addressed in section 3.3 appear as red zones on the map. Note that those circular red zones appear as ellipses here because of the Miller projection (a modified Mercator projection) used for drawing the map.

2. Volcanic Tremors at the Klyuchevskoy Volcanic Group

The Klyuchevskoy volcanic group (KVG) is one of the most active subduction-zone volcanic groups in the world. It consists of 13 stratovolcanoes located in an approximately 70-km-diameter zone on the Russian Kamchatka peninsula (Shapiro et al., 2017). Three volcanoes of the KVG (Klyuchevskoy, Bezymianny, and Tolbachik) were active during recent decades (e.g., Gordeev et al., 1989; Ivanov, 2008; Ozerov et al., 2007; Senyukov et al., 2009; Senyukov, 2013; Shapiro et al., 2017). In addition, two other very active volcanoes, Shiveluch and Kizimen, are respectively located north and south of KVG (Figure 1).

2.1. Single-Station Based Monitoring of Volcanic Tremors

The Kamchatka Branch of the Geophysical Survey of the Russian Academy of Sciences operates the permanent seismic network monitoring the KVG and surrounding volcanoes (Chebrov et al., 2013; Gordeev et al., 2006). In this paper, we use 4.5 years of seismic data continuously recorded between January 2009 and June 2013 by this permanent network composed of 18 stations in 2009 and 19 stations from 2010 onward. The stations and the five monitored volcanoes are shown in Figure 1. The seismic stations have three components,

each one being equipped by a CM-3 short-period seismometer with a corner frequency of around 0.8 Hz. Continuous records are sampled at 128 Hz, and only the vertical component is analyzed in this article, studied tremors being more energetic in the vertical direction (but horizontal components could also be used as mentioned in section 2.2.1).

As many volcanological observatories do all over the world, the Kamchatka Branch of the Geophysical Survey monitors volcanic tremors using a simple single-station approach. For example, stations LGN and KMN are used to monitor Klyuchevskoy and Tolbachik tremors, respectively (Figure 1). This simple approach suffers from limitations of robustness if the reference station breaks down, precision if electronic noise is confused with tremor, and impossibility to spatially locate the tremor.

2.2. Network-Based Monitoring of Volcanic Tremors

To overcome the limitations of single-station based approaches, we propose to use a network-based strategy that exploits the coherence of signals simultaneously recorded by several receivers. It is based on the network covariance matrix that can be used to extract coherent signals propagating across the network by reducing local noise (Seydoux et al., 2016). A detailed explanation of the covariance matrix estimation from real data is presented in section 2.2.1.

Being interested in long-duration tremors and not in short transient events, all inferences are obtained from day-long network covariance matrices. Once detected through the analysis of the daily network covariance matrix eigenvalues (please refer to section 2.2.2 for more information), different volcanic tremors can be clustered and located by using the daily network covariance matrix first eigenvector (section 2.2.3).

2.2.1. Estimation of the Daily Network Covariance Matrix

We here narrow the focus on the vertical-component records in our analysis, though an extension of this strategy to three-component data is possible (Wagner & Owens, 1995). We form the spectral network data vector $\mathbf{u}(f, t)$ from the records of the N seismic stations as

$$\mathbf{u}(f, t) = [u_1(f, t), u_2(f, t), \dots, u_N(f, t)]^T, \quad (1)$$

where $u_i(f, t)$ is the Fourier transform of the signal recorded at the station $i = 1 \dots N$ calculated over a time window of duration δt and starting at t .

The general workflow of covariance matrix estimation is summarized with the next steps:

1. Seismic data are downsampled from 128 Hz down to 25.6 Hz after bandpass-filtering between 0.1 and 10 Hz in order to allow for faster computation. We consider the raw data without correcting for the instrument response, because all the sensors are identical.
2. We apply spectral whitening to the seismic records (independently for every station) in order to enhance the coherence of the tremors signals (Bensen et al., 2007). Spectral whitening is often combined with temporal normalization in order to attenuate the amplitude of strong impulsive sources (earthquakes). But applied alone, as done here, the spectral whitening has shown to significantly improve the detection of volcanic tremors at Kamchatka (Soubestre et al., 2018). Indeed, it diminishes the influence of strong earthquakes and local noise and preserves the amplitude modulation of tremor signals, which is useful information when tremors are not fully stationary in time and rather represent sequences of many impulsive long-period events.
3. We divide the seismic data into time windows of duration δt from which the Fourier transform is calculated in order to obtain the spectral data vector (equation (1)). We also avoid artifacts caused by sharp windows by applying a tapering Hann window; we thus overlap the signal segments with a factor of 50% in order not to lose any information located in consecutive windows.
4. We calculate the covariance matrix from sets of M consecutive overlapping segments of data, such as

$$\mathbf{C}(f, t) = \langle \mathbf{u}(f, t) \mathbf{u}^\dagger(f, t) \rangle_{\Delta t} = \frac{1}{M} \sum_{m=0}^{M-1} \mathbf{u}(f, t + m\delta t/2) \mathbf{u}^\dagger(f, t + m\delta t/2). \quad (2)$$

5. The covariance matrix $\mathbf{C}(f, t)$ is then obtained for each time t and incorporates information about the data collected in the interval $[t, t + \Delta t]$ where $\Delta t = (1 + M)\delta t/2$. We decide to calculate the covariance matrix with a sliding step of $\Delta t/4$ in order to have an appreciable final temporal resolution in our analysis.
6. The daily covariance matrix is finally obtained by averaging consecutive covariance matrices obtained within 1 day of data. Note that this windowing and averaging is necessary because a matrix built from

day-long spectra (without windowing) would be generated from a single data vector. Inherently, with such a matrix being of rank one, only a single eigenvector could be obtained. In order to observe the splitting of different sources onto different eigenvectors, we must average the wavefield observations onto smaller windows, allowing to increase the rank of the covariance matrix and to better separate sources.

As this daily network covariance matrix is inherently Hermitian and positive semidefinite (Seydoux et al., 2016), it can be decomposed on the basis of its complex eigenvectors $\mathbf{v}^{(i)}$ associated with real positive eigenvalues λ_i :

$$\mathbf{C}(f, t) = \sum_{i=1}^N \lambda_i(f, t) \mathbf{v}^{(i)}(f, t) \mathbf{v}^{(i)\dagger}(f, t). \quad (3)$$

2.2.2. Detection of Tremors From the Covariance Matrix Eigenvalues

According to Seydoux, Shapiro, de Rosny, Brenguier, and Landès (2016), the number of nonzero eigenvalues is related to the number of statistically independent signals composing the wavefield and then of independent seismic sources. Real seismic data are composed of a large amount of seismic sources ranging from earthquakes and tremors to more complex sources usually designated as noise sources (hum, oceanic microseisms, wind, anthropic activity, scatterers acting like secondary sources, self-sensor electronic noise, etc). This large number of sources are not absolutely independent and may be located onto similar eigenvectors. Also, the estimation of the covariance matrix from a finite number of windows may also reduce our ability to capture the independent seismic signals. For these reasons, deriving the exact number of independent sources is a challenge (e.g., Wax & Kailath, 1985) that is out of scope in the present study. Nevertheless, an estimate of the “level of coherence” of the seismic wavefield can be obtained by calculating the width $\sigma(f, t)$ of the covariance matrix eigenspectrum (the covariance matrix *spectral width*), a proxy for the presence of coherent signal within the seismic wavefield:

$$\sigma(f, t) = \frac{\sum_{i=1}^N (i-1) \lambda_i(f, t)}{\sum_{i=1}^N \lambda_i(f, t)}. \quad (4)$$

This spectral width can be seen as a proxy for the number of independent seismic sources. Thus, the spectral width corresponding to ambient seismic noise produced by distributed noise sources is high, whereas the spectral width of a signal spatially coherent at the network scale generated by a single localized source is low.

The spectral width $\sigma(f, t)$ computed from daily covariance matrices during the 4.5-years-long studied time period is analyzed by Soubestre et al. (2018). This result clearly shows three main long-duration episodes when the spectral width is reduced: (1) in the beginning of 2009, (2) from the end of 2009 to the end of 2010, and (3) from the end of 2012 to mid-2013. From a priori knowledge (Droznin et al., 2015), we know that the two first episodes correspond to periods of strong noneruptive tremors at Klyuchevskoy and the last one to a strong eruptive tremor at Tolbachik. This approach based on eigenvalues is therefore efficient to detect volcanic tremor, but it is unable to tell whether those detected tremor sources are from the same volcano or from different ones (here we know it from a priori knowledge). To overcome the limitation of this approach to distinguish different sources of volcanic tremor, section 2.2.3 focuses on the eigenvectors of the daily network covariance matrix.

2.2.3. Clustering and Location of Tremors From the Covariance Matrix First Eigenvector

Instead of using directly the daily network covariance matrix to cluster or locate tremor sources, it has been shown in Soubestre et al. (2018) that better results are obtained by using the covariance matrix first eigenvector. The idea is derived from principal component analysis, where the first component (eigenvector) is known to represent the most coherent part of the wavefield (Seydoux et al., 2016; Wagner & Owens, 1995). Therefore, for days with tremor activity, the first eigenvector characterizes the dominant tremor source and acts as a denoising operator because the higher-order eigenvectors are orthogonal to the first one and most likely span information related to the background noise. It has to be noticed that such a filtering by the first eigenvector theoretically avoids the possibility of identifying simultaneously active tremor sources from different volcanoes. Being mainly interested by the daily dominating tremor source in the studied region, this is not a problem for our purpose. But further work should be realized to analyze in detail periods when

more than one volcano are emitting tremor simultaneously, which is out of scope of the present article. This distinction of simultaneously acting tremors might require to include higher-order eigenvectors of the covariance matrix in the analysis. Another option could be to consider horizontal components, in order to bring polarization constraint in the analysis (Vidale, 1986).

The frequency-dependent first eigenvector of the daily covariance matrix $\mathbf{V}_1(\text{day}, f)$ can be analyzed to cluster and/or locate the daily dominant tremor source. Using a correlation coefficient as a measure of their similarity, Soubestre et al. (2018) developed a clustering algorithm to analyze this collection of daily first eigenvectors. The clustering process identifies seven clusters associated with seismovolcanic activity during the time period considered in the present article. Each cluster's central day eigenvector (highest correlation coefficient) corresponds to the most characteristic first eigenvector of the cluster. Those characteristic eigenvectors can then be used as templates for template matching detection of tremor sources, comparing them with the daily first eigenvectors from the continuous records (Droznin et al., 2015) or with new available data. This clustering approach is interesting to classify different sources of volcanic tremor, but it does not associate the obtained clusters to volcanoes of the studied zone. This location of tremors can be done using the moveout information of the daily first eigenvector, as detailed in the next section.

3. Automatic 3-D Location of Volcanic Tremor Sources

Methods of volcanic tremor sources location from network cross correlations have already been proposed in previous studies (e.g., Ballmer et al., 2013; Barriere et al., 2017; Donaldson et al., 2017; Droznin et al., 2015; Li et al., 2016, 2017; Woods et al., 2018; Yukutake et al., 2017), but with an a priori on the type of wave emerging in cross correlations. Because they study shallow tremor sources, the authors assume that cross correlations are dominated by surface waves. Conversely to those methods considering a surface wave propagation from the tremor source, the cross-correlations-based location method developed in our article assumes an S wave propagation and the knowledge of the associated S wave structure, allowing to locate shallow as well as deep tremor sources. Another main difference between the method proposed here and existing ones is that the considered cross correlations are not directly those of the interstations cross-correlations matrix, but those derived from the first eigenvector of the network covariance matrix. This makes the cross correlations more representative of the dominant tremor, as proved in the supporting information Text S1 where the location of a synthetic tremor (made of multiple long-period events merging) is more precisely recovered using the filtering of the network covariance matrix by its first eigenvector than the full matrix itself.

3.1. Method: 3-D Location From Cross-Correlations Envelopes

Volcanic tremor sources can be located using the moveout information contained in the daily network covariance matrix first eigenvector, that contains information about the location and the mechanism of the dominating tremor source. We extract the filtered covariance matrix $\tilde{\mathbf{C}}(f, t)$ from the complex outer product of the first eigenvector $\mathbf{v}^{(1)}(f, t)$ with its Hermitian transpose

$$\tilde{\mathbf{C}}(f, t) = \mathbf{v}^{(1)}(f, t) \mathbf{v}^{(1)\dagger}(f, t). \quad (5)$$

This operation can be seen as a low-rank denoising of the covariance matrix, a strategy widely used in image processing to remove the noise spanned by higher-order eigenvectors (Orchard et al., 2008). The inverse Fourier transform of this matrix retrieves the time-domain filtered cross correlations:

$$\tilde{\mathbf{R}}(\tau, t) = \mathcal{F}^{-1} \tilde{\mathbf{C}}(f, t), \quad (6)$$

where \mathcal{F}^{-1} is the inverse Fourier transform operated to the frequency dimension, and τ is the cross-correlation time lag.

To locate the position of the dominant tremor source, we use a grid search on a 3-D space grid. We compute covariance matrices (5) at frequencies between 0.5 and 2.0 Hz (spectral band where tremors are more energetic in Kamchatka according to Droznin et al., 2015 and Soubestre et al., 2018). The resulting time-domain cross correlations are naturally filtered in the same range. We then compute the smooth envelope of the cross-correlations $\mathbf{E}(\tau, t)$ by computing the absolute value of the analytic signal derived from the Hilbert transform h and performing a convolution with a Gaussian filter $g(t)$ with a 100-s width:

$$\mathbf{E}(\tau, t) = g(t) \otimes |\tilde{\mathbf{R}}(\tau, t) + ih(\tilde{\mathbf{R}})(\tau, t)|, \quad (7)$$

where $g(t) = \frac{1}{\beta\sqrt{2\pi}} \exp\left(-\frac{1}{2} \frac{t^2}{\beta^2}\right)$ is a Gaussian window with typical width $\beta = 10$ s (larger values have been tested with no significant difference, and the $\beta = 10$ s value was found to be the best lower bound). The smoothing operation allows to reduce the alteration of the location quality from scattering due to local heterogeneities and from the imprecision of the location method itself, particularly the imprecision of the velocity model described hereafter.

Then, for every point $\mathbf{r} = x\mathbf{e}_x + y\mathbf{e}_y + z\mathbf{e}_z$ of the 3-D grid, each cross-correlation envelope $E_{ij}(\tau)$ is shifted by the time difference $d\tau_{ij}(\mathbf{r})$ between travel times needed for an S wave to travel from the tested point to the two stations i and j :

$$d\tau_{ij}(\mathbf{r}) = \tau_i(\mathbf{r}) - \tau_j(\mathbf{r}). \quad (8)$$

Travel times $\tau_i(\mathbf{r})$ and $\tau_j(\mathbf{r})$ are calculated based on the 1-D velocity model for S waves (dominating in volcanic tremors) accounting for velocity variation with depth derived by Droznina et al. (2017), described in supporting information Text S2. The value at zero lag-time of shifted cross-correlations envelopes is finally stacked for all station pairs to obtain the network response function, and this computation is repeated for every day starting at time t :

$$b(\mathbf{r}, t) = \sum_{i=1}^N \sum_{j>i}^N E_{ij}(-d\tau_{ij}(\mathbf{r}), t). \quad (9)$$

Note that, cross-correlations envelopes being not relatively normalized, the weight in the stack of the network response of each individual cross-correlation envelope is directly related to its quality (spiky shape).

The grid search is performed on a grid covering the whole studied zone down to 50-km depth, with a $1 \text{ km} \times 1 \text{ km} \times 1 \text{ km}$ resolution. In order to compare relative levels of tremor between different days, each daily network response function $b(\mathbf{r}, t)$ is normalized first by its integral on the total grid volume V :

$$\ell(\mathbf{r}, t) = \frac{b(\mathbf{r}, t)}{\int_V b(\mathbf{r}, t) d\mathbf{r}}. \quad (10)$$

Then, those spatially normalized response functions are temporally renormalized by the maximum of the whole time period:

$$\tilde{\ell}(\mathbf{r}, t) = \frac{\ell(\mathbf{r}, t)}{\max_t \ell(\mathbf{r}, t)}. \quad (11)$$

As the integral-normalized network response (10) sums to unity on the total grid volume, it can be referred to as a presence likelihood of the tremor source. Similarly, the renormalized response (11) represents this presence likelihood relatively to the maximum likelihood of the considered period. The most likely daily source position corresponds to the maximum of this function in space.

3.2. Results: 3-D Location of Volcanic Tremors

Figure 2 shows examples of renormalized network response function (11) for selected days. Most probable daily tremor source location is marked by a black star. This figure clearly shows that during the studied time period, volcanic tremors are originating from different volcanoes or from different activity phases of a particular volcano. Thus, Figure 2a shows a day of quite deep tremor activity beneath Shiveluch volcano. Figures 2b and 2c respectively correspond to a deep and a shallow tremor activity beneath Klyuchevskoy. Figures 2d and 2f respectively show days of shallow tremor activity beneath Kizimen and Tolbachik. Finally, a response function corresponding to a day during the calm period in 2012 without tremor activity, but maybe dominated by a regional earthquake, appears in Figure 2e for comparison. For more information, supporting information Text S3 shows cross-correlations envelopes corresponding to Figures 2c and 2e.

If some days correspond to shallow tremor sources (Figures 2c, 2d, and 2f), other days such as 2009-088 of Figure 2a and 2009-276 of Figure 2b are showing a deep tremor source. This result is quite interesting, because it is the first time that a deep volcanic tremor is located by a cross-correlation-based method. It means that during those days, the located volcanic tremor has a source associated with body waves. In the context of the KVG, those body waves are emitted by volcanic tremor sources located in the consolidated

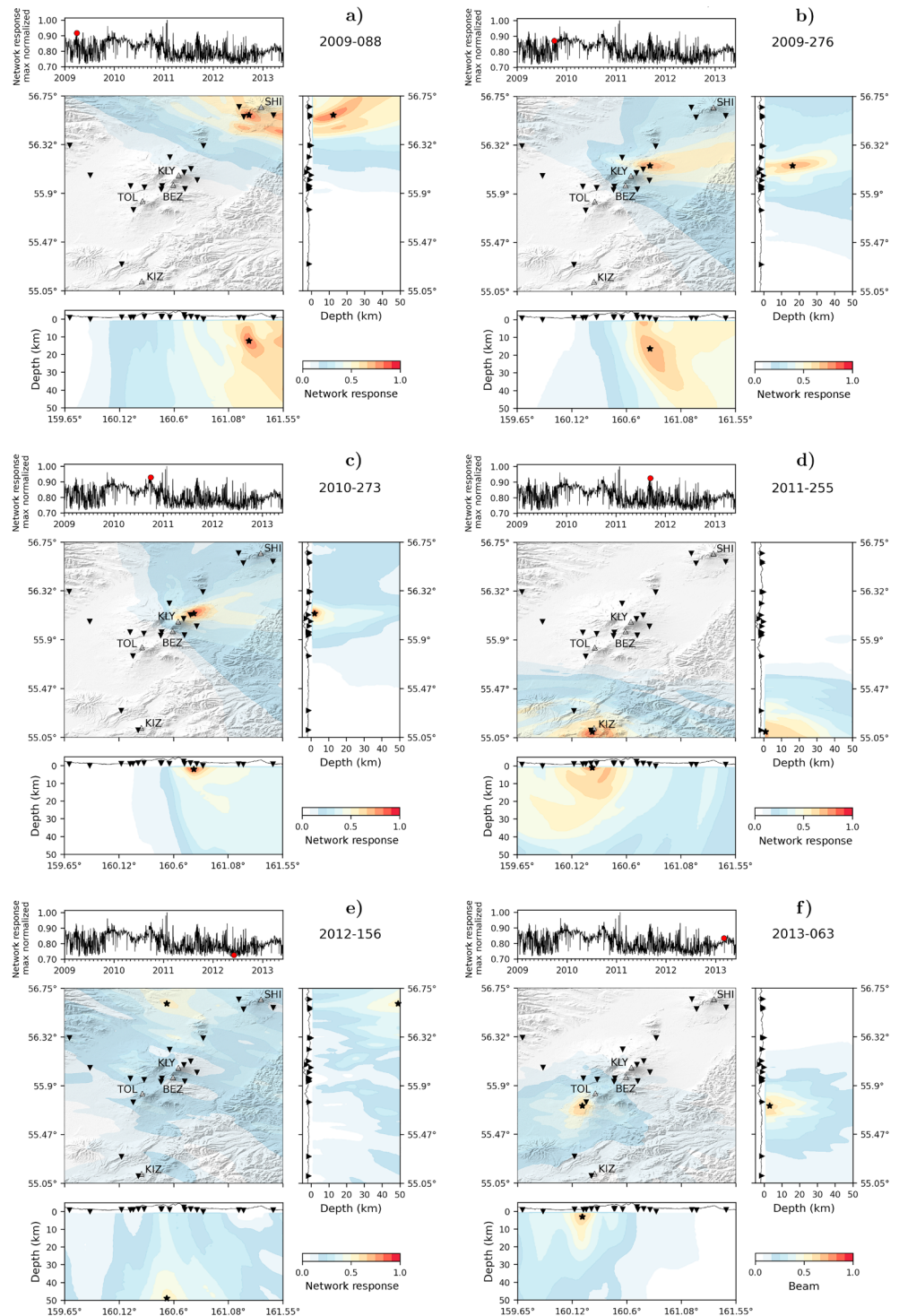


Figure 2. Volcanic tremor source presence likelihood (corresponding to (11)) corresponding to six different days (red dot in top left black curves). On each response function, the most probable tremor source location is marked by a black star. Each response function appears as a top view of its values in the horizontal plane corresponding to the depth of the tremor source (center panel) and two side views of its values in vertical planes corresponding respectively to the depth-longitude plane (bottom panel) and the depth-latitude plane (right panel) of the tremor source. Seismic stations and volcanoes respectively appear as black inverted triangles and with triangles in the horizontal top view (center panel), and the first three initial letters of each volcano help the reader to orient. (a) Quite deep tremor beneath Shiveluch on day 2009-088. (b) Deep tremor beneath Klyuchevskoy on day 2009-276. (c) Shallow tremor beneath Klyuchevskoy on day 2010-273. (d) Shallow tremor beneath Kizimen on day 2011-255. (e) Calm period without tremor activity on day 2012-156. (f) Shallow tremor beneath Tolbachik on day 2013-063.

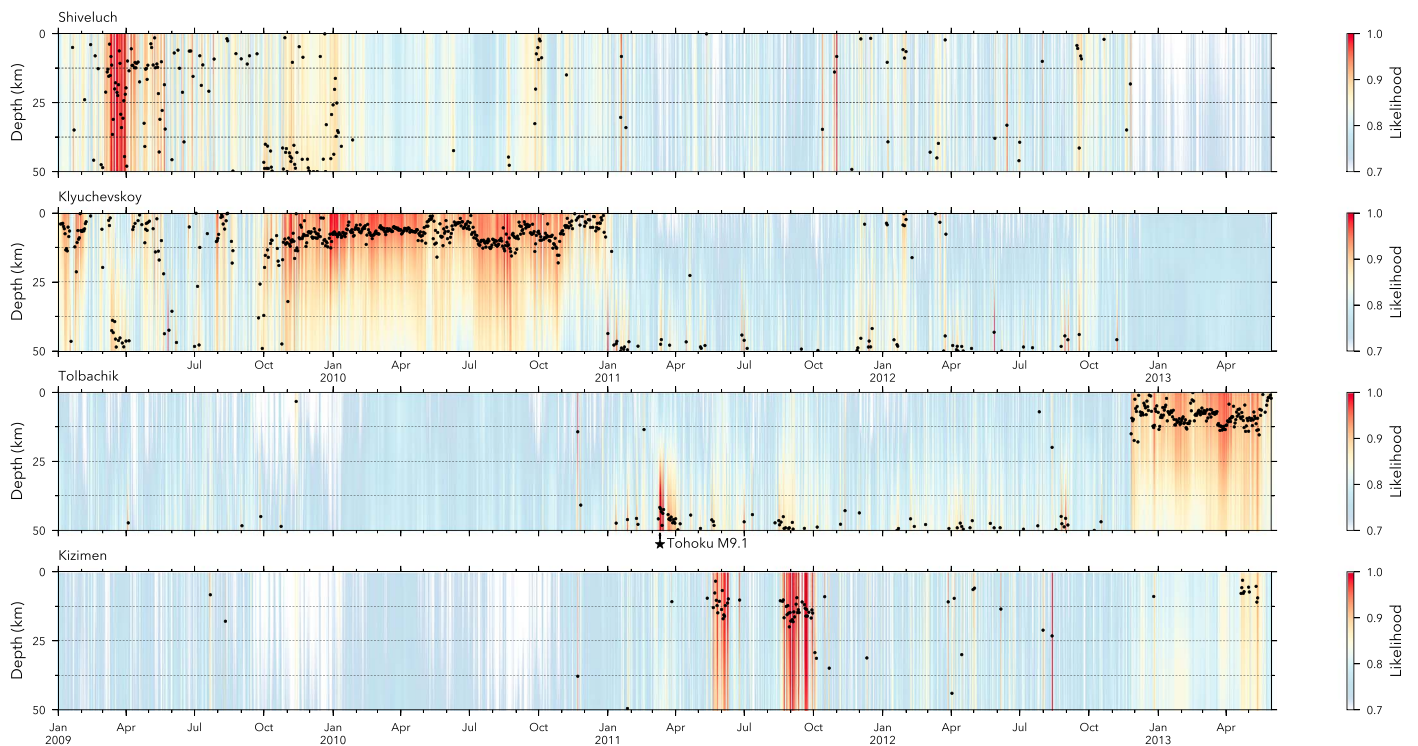


Figure 3. Time evolution of tremor sources depth beneath each studied volcano (Shiveluch, Klyuchevskoy, Tolbachik, and Kizimen from north to south). A circular zone of radius $r = 25$ km is defined around each volcano (the zone is centered on volcanoes summit as appearing in Figure 1), and the maximum value of the likelihood (11) over those circular zones is selected at every depth and every day. The expected value \bar{z} of the likelihood for each zone and each time is calculated with $\bar{z}(t) = \int \max_{x,y} \ell(\sqrt{x^2 + y^2} < r, z, t) z dz$ and represented as a black dot in order to better visualize the expected position of the tremor sources. The time of the 2011 M9.1 Tohoku earthquake (Ozawa et al., 2011) is indicated with a black star beneath the results from the Tolbachik volcano.

bedrock under unconsolidated sedimentary or volcanic deposits. Note that such an emergence of body waves in cross correlations has already been observed in other different contexts and scales, such as body waves propagating through the active magmatic system of the Piton de la Fournaise volcano (Nakata et al., 2016), body waves reflected from the Moho (Poli, Pedersen, et al. 2012), or body waves from the mantle transition zone (Poli, Campillo, et al. 2012).

3.3. Results: Time Evolution of Volcanic Tremor Sources 3-D Location

The issue of the vertical migration of volcanic tremor sources with time is addressed here. The tremor presence likelihood (11) is daily analyzed beneath each studied volcano (Shiveluch, Klyuchevskoy, Tolbachik, and Kizimen from north to south) to check for the source depth. To do so, a circular zone of a given radius is defined around each volcano (the zone is centered on volcanoes summit as appearing in Figure 1) and the maximum value of the likelihood (11) over those circular zones is selected at every depth and every day. The expected value \bar{z} of the likelihood for each zone and each time is calculated with $\bar{z}(t) = \int \max_{x,y} \ell(\sqrt{x^2 + y^2} < r, z, t) z dz$ and represented as a black dot in order to better visualize the expected position of the tremor sources. Figure 3 shows the result of such an analysis for 25-km radius zones, as shown in Figure 1. Note that the likelihood has been clipped below a value of 0.7 in order to narrow the focus on the highly coherent time segments.

This time-depth analysis clearly enhances the same time periods of tremor activity as the detection of tremors by Droznin et al. (2015) and Soubestre et al. (2018), but with the benefit that here each tremor is clearly associated to a specific volcano. Disregarding the depth information and looking only at the time axis of Figure 3, this result showing when each volcano is under tremor is interesting from a monitoring point of view and this approach could be usefully run in real time in a volcanological observatory. Thus, volcanic tremor activity is automatically located at Shiveluch volcano in March 2009, at Klyuchevskoy volcano at the beginning of 2009 and also from September 2009 to the end of 2010, at Kizimen during two episodes of one month in June and September 2011, and at Tolbachik volcano from the end of November 2012 onward. We

also see that during periods of volcanic rest (e.g., March 2011) the likelihood presence is the highest at great depth and is most likely related to strong earthquakes that resisted our preprocessing; this is mostly due to the presence of dominating body waves in the seismic wavefield at global scales usually observed after big events (Boué et al., 2014; Sens-Schönfelder et al., 2015). For example in this period, the *M*9.1 Tohoku earthquake (Ozawa et al., 2011) is clearly visible on our results for several days (Figure 3, beneath the Tolbachik inset).

Moreover, the depth of the daily dominating tremor source is made better visible by Figure 3. Looking at the spatial distribution of volcanoes and seismic stations in the map of Figure 1, one understands that the source depth is not well constrained at volcanoes Shiveluch and Kizimen that are located at the border of the studied zone and count with a few stations. Likewise, Tolbachik volcano is more central in the map but it counts only one station close to it, so that the depth estimation of tremor sources beneath Tolbachik cannot be very precise. Figure 3 shows that Tolbachik's tremor is an eruptive tremor, beginning on 27 November 2012 one day after the official beginning of the fissure eruption that started on 26 November. Looking at Figure 2f, the tremor source seems to be superficial. This result is consistent with the analysis from Caudron et al. (2015) who relate this eruptive tremor to lava flows. This is not surprising for this tremor to be superficial given that the seismic preparatory phase of Tolbachik's 2012–2013 eruption was also shallow. Indeed, the eruption was preceded by 4–5 months of shallow (depth < 5 km) and low-energy volcano-tectonic seismicity (Kugaenko et al., 2015), as well as shallow long-period events clustered in time due to multiple cracks and channels reactivation (Frank et al., 2018). The eruption is supposed to have been fed by magma ascending from a shallow crustal magma storage (Fedotov et al., 2010, 2011).

On the other hand, the depth of tremor sources is better constrained for Klyuchevskoy volcano that is central in the map and count multiple stations around it. Moreover, the plumbing system of Klyuchevskoy is known to be more complex and to contain deeper levels of magma storage, as evidenced by different types of studies. Thus, Koulakov et al. (2011) imaged a crustal storage beneath Klyuchevskoy at intermediate depth of 8–13 km and a deeper one in the mantle below 25-km depth. This latter deep storage was also identified by analysis of deep long-period earthquakes (Shapiro et al., 2017). In Figure 3, the 2009–2010 preeruptive tremor of Klyuchevskoy volcano seems to affect shallow (depth < 5 km), medium (5 km < depth < 15 km), and greater depths of about 20–25 km at the beginning of the time period. The tremor shows different phases from September 2009 to December 2010. First, from September to December 2009, the expected position of the tremor source (black dots in Figure 3) progressively migrates from great depths of about 25 km to medium depths of 10 km. Then, the tremor activity seems to stabilize around 10 km from January to June 2010, when it starts to focus to shallower depths of a few kilometres. At the beginning of July 2010 the expected position of the tremor source starts to move deeper again down to 15 km, where it stabilizes up to the end of October 2010. This change could be interpreted as a possible reinjection of magma from a deep reservoir. And eventually, from November 2010 onward the dominant tremor source progressively migrates to the surface, a few months before the beginning of the summit eruption that started in December 2010. This evidence of the sequence of dominant tremor source depth decrease with time getting closer to the eruption is an interesting result consistent with the dynamics of magmatic eruption processes.

4. Conclusion

In this paper, we developed a cross-correlations-based method to automatically locate volcanic tremor sources in 3-D. The method consists in a first preprocessing step to normalize the data and calculate the daily network covariance matrix, a second step of filtering this matrix by its first eigenvector to retrieve the daily dominant tremor source, and a last step to locate this source from the moveout information of the first eigenvector. An important aspect of the developed method is that once the *S* wave velocity model and all parameters are selected, the data analysis and the following detection and location of tremor sources are fully automatic without need of additional a priori information. A main difference between the developed cross-correlations-based location method of volcanic tremor and other existing ones is that instead of assuming a surface wave-type propagation and a shallow origin of the tremor, we estimate the tremor source depth and we are able to locate shallow as well as deep tremors. Another main difference is that the considered cross correlations are not directly those of the interstations cross-correlations matrix but those derived from the first eigenvector of the network covariance matrix that characterizes the dominant component of the recorded wavefield.

The daily application of the developed method onto 4.5 years of data (from January 2009 to June 2013) from the Klyuchevskoy group of volcanoes allowed to daily locate the dominant volcanic tremor source, which is interesting from the monitoring point of view of a volcanological observatory. It also enabled to track the temporal evolution of the 3-D location of the preeruptive volcanic tremor beneath Klyuchevskoy from deep to shallow parts of the plumbing system, from September 2009 to December 2010 when the summit eruption started. This latter result is interesting, first because to our knowledge it is the first time a deep volcanic tremor source is located with a cross-correlation-based method and second because the evolution of the tremor source depth during 1.5 years including preeruptive and coeruptive activity is quite nicely recovered. According to the analysis, initially multiple tremor sources are acting simultaneously from the surface to depths down to 20–25 km, and then the dominating tremor source progressively migrates to the surface. This surface migration pattern is observed twice during the 2009–2010 tremor of Klyuchevskoy, first from September 2009 to the end of June 2010 and second from mid-July to December 2010 after a possible reinjection in July–August. This behavior of volcanic tremor sources affecting a wide depth range and then migrating to the surface can be explained by the model proposed by Stasiuk et al. (1993) of progressive magma draining from the bottom of vertical pathways during eruptions.

Acknowledgments

This study was financially supported by the project VOLRISKMAC (MAC/3.5b/124) cofinanced by the European Union MAC 2014–2020 Cooperation Transnational Programs, by the project TFvolcano financed by the Program Tenerife Innova 2016–2021 coordinated by the Tenerife 2030 Area of the Cabildo Insular de Tenerife, by the Russian Ministry of Education and Science (grant N 14.W03.31.0033), and by the European Research Council (ERC) under the European Union Horizon 2020 Research and Innovation Programme (grant agreement 787399-SEISMAZE). Computations were performed using the infrastructure of the Institute of Volcanology and Seismology and of the Kamchatka Branch of the Geophysical Survey, as well as the IGP High-Performance Computing infrastructure S-CAPAD (supported by the Ile-de-France region via the SEASAME programme, by France-Grille, and by the CNRS MASTODONS programme). Seismological time series used for the analysis are available from the Kamchatka Branch of the Geophysical Survey of Russian Academy of Sciences (<http://www.emsd.ru>) on request.

References

- Aki, K., & Koyanagi, R. (1981). Deep volcanic tremor and magma ascent mechanism under Kilauea, Hawaii. *Journal of Geophysical Research*, 86(B8), 7095–7109. <https://doi.org/10.1029/JB086iB08p07095>
- Almendros, J., Abella, R., Mora, M. M., & Lesage, P. (2014). Array analysis of the seismic wavefield of long-period events and volcanic tremor at Arenal Volcano, Costa Rica. *Journal of Geophysical Research: Solid Earth*, 119, 5536–5559. <https://doi.org/10.1002/2013JB010628/full>
- Almendros, J., Ibáñez, J., Alguacil, G., Del Pezzo, E., & Ortiz, R. (1997). Array tracking of the volcanic tremor source at Deception Island, Antarctica. *Geophysical Research Letters*, 24(23), 3069–3072. <https://doi.org/10.1029/97GL03096>
- Almendros, J., Ibáñez, J. M., Carmona, E., & Zandomenighi, D. (2007). Array analyses of volcanic earthquakes and tremor recorded at Las Cañadas caldera (Tenerife Island, Spain) during the 2004 seismic activation of Teide Volcano. *Journal of Volcanology and Geothermal Research*, 160(3), 285–299. <https://doi.org/10.1016/j.jvolgeores.2006.10.002>
- Ballmer, S., Wolfe, C. J., Okubo, P. G., Haney, M. M., & Thurber, C. H. (2013). Ambient seismic noise interferometry in Hawai'i reveals long-range observability of volcanic tremor. *Geophysical Journal International*, 194, ggt112. <https://doi.org/10.1093/gji/ggt112>
- Barriere, J., Oth, A., Theys, N., d'Oreye, N., & Kervyn, F. (2017). Long-term monitoring of long-period seismicity and space-based SO₂ observations at African lava lake volcanoes Nyiragongo and Nyamulagira (DR Congo). *Geophysical Research Letters*, 44, 6020–6029. <https://doi.org/10.1002/2017GL073348>
- Battaglia, J., Aki, K., & Ferrazzini, V. (2005). Location of tremor sources and estimation of lava output using tremor source amplitude on the Piton de la Fournaise Volcano: 1. Location of tremor sources. *Journal of Volcanology and Geothermal Research*, 147(3), 268–290. <https://doi.org/10.1016/j.jvolgeores.2005.04.005>
- Bensen, G., Ritzwoller, M., Barmin, M., Levshin, A., Lin, F., Moschetti, M., et al. (2007). Processing seismic ambient noise data to obtain reliable broad-band surface wave dispersion measurements. *Geophysical Journal International*, 169(3), 1239–1260.
- Boué, P., Poli, P., Campillo, M., & Roux, P. (2014). Reverberations, coda waves and ambient noise: Correlations at the global scale and retrieval of the deep phases. *Earth and Planetary Science Letters*, 391, 137–145.
- Caudron, C., Taisne, B., Kugaenko, Y., & Saltykov, V. (2015). Magma migration at the onset of the 2012–13 Tolbachik eruption revealed by seismic amplitude ratio analysis. *Journal of Volcanology and Geothermal Research*, 307, 60–67.
- Chebrov, V., Droznin, D., Kugaenko, Y. A., Levina, V., Senyukov, S., Sergeev, V., et al. (2013). The system of detailed seismological observations in Kamchatka in 2011. *Journal of Volcanology and Seismology*, 7(1), 16–36. <https://doi.org/10.1134/S0742046313010028>
- Chouet, B. A. (1996). Long-period volcano seismicity: Its source and use in eruption forecasting. *Nature*, 380(6572), 309–316.
- Chouet, B. A., & Matoza, R. S. (2013). A multi-decadal view of seismic methods for detecting precursors of magma movement and eruption. *Journal of Volcanology and Geothermal Research*, 252, 108–175. <https://doi.org/10.1016/j.jvolgeores.2012.11.013>
- Chouet, B., Saccorotti, G., Martini, M., Dawson, P., De Luca, G., Milana, G., & Scarpa, R. (1997). Source and path effects in the wave fields of tremor and explosions at Stromboli Volcano, Italy. *Journal of Geophysical Research*, 102(B7), 15,129–15,150.
- Ciaramella, A., De Lauro, E., Falanga, M., & Petrosino, S. (2011). Automatic detection of long-period events at Campi Flegrei caldera (Italy). *Geophysical Research Letters*, 38, L18302. <https://doi.org/10.1029/2011GL049065>
- Di Grazia, G., Falsaperla, S., & Langer, H. (2006). Volcanic tremor location during the 2004 Mount Etna lava effusion. *Geophysical research letters*, 33, L04304. <https://doi.org/10.1029/2005GL025177>
- Donaldson, C., Caudron, C., Green, R. G., Thelen, W. A., & White, R. S. (2017). Relative seismic velocity variations correlate with deformation at Kilauea Volcano. *Science Advances*, 3(6), e1700219. <https://doi.org/10.1126/sciadv.1700219>
- Droznin, D., Shapiro, N., Droznina, S. Y., Senyukov, S., Chebrov, V., & Gordeev, E. (2015). Detecting and locating volcanic tremors on the Klyuchevskoy group of volcanoes (Kamchatka) based on correlations of continuous seismic records. *Geophysical Journal International*, 203(2), 1001–1010. <https://doi.org/10.1093/gji/ggv342>
- Droznina, S. Y., Shapiro, N. M., Droznin, D. V., Senyukov, S. L., Chebrov, V. N., & Gordeev, E. I. (2017). S-wave velocity model for several regions of the Kamchatka Peninsula from the cross correlations of ambient seismic noise. *Physics of the Solid Earth*, 53(3), 341–352.
- Eibl, E. P., Bean, C. J., Jónsdóttir, I., Höskuldsson, A., Thordarson, T., Coppola, D., et al. (2017). Multiple coincident eruptive seismic tremor sources during the 2014–2015 eruption at Holuhraun, Iceland. *Journal of Geophysical Research: Solid Earth*, 122, 2972–2987. <https://doi.org/10.1002/2016JB013892/full>
- Eibl, E. P., Bean, C. J., Vogfjörð, K. S., Ying, Y., Lokmer, I., Möllhoff, M., et al. (2017). Tremor-rich shallow dyke formation followed by silent magma flow at Bar[eth]arbunga in Iceland. *Nature Geoscience*, 10(4), 299.
- Fedotov, S., Utkin, I., & Utkina, L. (2011). The peripheral magma chamber of Ploskii Tolbachik, a Kamchatka basaltic volcano: Activity, location and depth, dimensions, and their changes based on magma discharge observations. *Journal of Volcanology and Seismology*, 5(6), 369–385. <https://doi.org/10.1134/S0742046311060042>

- Fedotov, S., Zharinov, N., & Gontovaya, L. (2010). The magmatic system of the Klyuchevskaya group of volcanoes inferred from data on its eruptions, earthquakes, deformation, and deep structure. *Journal of Volcanology and Seismology*, 4(1), 1–33. <https://doi.org/10.1134/S074204631001001X>
- Fee, D., Steffke, A., & Garces, M. (2010). Characterization of the 2008 Kasatochi and Okmok eruptions using remote infrasound arrays. *Journal of Geophysical Research*, 115, D00L10. <https://doi.org/10.1029/2009JD013621>
- Firstov, P., & Shakirova, A. (2014). Seismicity observed during the precursory process and the actual eruption of Kizimen Volcano, Kamchatka in 2009–2013. *Journal of Volcanology and Seismology*, 8(4), 203–217. <https://doi.org/10.1134/S0742046314040022>
- Frank, W., & Shapiro, N. (2014). Automatic detection of low-frequency earthquakes (LFEs) based on a beamformed network response. *Geophysical Journal International*, 197(2), 1215–1223.
- Frank, W. B., Shapiro, N. M., & Gusev, A. A. (2018). Progressive reactivation of the volcanic plumbing system beneath Tolbachik Volcano (Kamchatka, Russia) revealed by long-period seismicity. *Earth and Planetary Science Letters*, 493, 47–56. <https://doi.org/10.1016/j.epsl.2018.04.018>
- Goldstein, P., & Chouet, B. (1994). Array measurements and modeling of sources of shallow volcanic tremor at Kilauea Volcano, Hawaii. *Journal of Geophysical Research*, 99(B2), 2637–2652.
- Gordeev, E., Chebrov, V., Levina, V., Senyukov, S., Shevchenko, Y. V., & Yashchuk, V. (2006). The system of seismological observation in Kamchatka, Vulkanol. Seismol.
- Gordeev, E., Melnikov, Y. Y., Sinitsyn, V., & Chebrov, V. (1989). Volcanic tremor of Kliuchevskoi Volcano (1984 eruption). In *Volcanic hazards* (pp. 486–503). Berlin, Heidelberg: Springer.
- Gordeev, E., Murav'ev, Y. D., Samoilenko, S., Volynets, A., Mel'nikov, D., & Dvigalo, V. (2013). The Tolbachik fissure eruption of 2012–2013: Preliminary results. *Doklady Earth Sciences*, 452, 1046–1050. <https://doi.org/10.1134/S1028334X13100103>
- Han, J., Vidale, J. E., Houston, H., Schmidt, D., & Creager, K. C. (2018). Deep long-period earthquakes beneath Mount St. Helens: Their relationship to tidal stress, episodic tremor and slip, and regular earthquakes. *Geophysical Research Letters*, 45, 2241–2247. <https://doi.org/10.1002/2018GL077063>
- Haney, M. M. (2010). Location and mechanism of very long period tremor during the 2008 eruption of Okmok Volcano from interstation arrival times. *Journal of Geophysical Research*, 115, B00B05. <https://doi.org/10.1029/2010JB007440>
- Hasegawa, A., Zhao, D., Hori, S., Yamamoto, A., & Horiuchi, S. (1991). Deep structure of the northeastern Japan arc and its relationship to seismic and volcanic activity. *Nature*, 352(6337), 683–689. <https://doi.org/10.1038/352683a0>
- Hotovec-Ellis, A. J., Shelly, D. R., Hill, D. P., Pitt, A. M., Dawson, P. B., & Chouet, B. A. (2018). Deep fluid pathways beneath Mammoth Mountain, California, illuminated by migrating earthquake swarms. *Science Advances*, 4(8), eaat5258. <https://doi.org/10.1126/sciadv.aat5258>
- Ichimura, M., Yokoo, A., Kagiya, T., Yoshikawa, S., & Inoue, H. (2018). Temporal variation in source location of continuous tremors before ash–gas emissions in January 2014 at Aso Volcano, Japan. *Earth, Planets and Space*, 70(1), 125. <https://doi.org/10.1186/s40623-018-0895-4>
- Ivanov, V. (2008). Current cycle of the Kluchevskoy Volcano activity in 1995–2008 based on seismological, photo, video and visual data. In *Proceedings of conference, petropavlovsk-kamchatsky* (pp. 27–29).
- Iverson, R. M., Dzurisin, D., Gardner, C. A., Gerlach, T. M., LaHusen, R. G., Lisowski, M., et al. (2006). Dynamics of seismogenic volcanic extrusion at Mount St Helens in 2004–05. *Nature*, 444(7118), 439–443. <https://doi.org/10.1038/nature0532>
- Jolly, A., Lokmer, I., Thun, J., Salichon, J., Fry, B., & Chardot, L. (2017). Insights into fluid transport mechanisms at White Island from analysis of coupled very long-period (VLP), long-period (LP) and high-frequency (HF) earthquakes. *Journal of Volcanology and Geothermal Research*, 343, 75–94. <https://doi.org/10.1016/j.jvolgeores.2017.06.006>
- Kao, H., & Shan, S.-J. (2004). The source-scanning algorithm: Mapping the distribution of seismic sources in time and space. *Geophysical Journal International*, 157(2), 589–594.
- Konstantinou, K. I., & Schlindwein, V. (2003). Nature, wavefield properties and source mechanism of volcanic tremor: A review. *Journal of Volcanology and Geothermal Research*, 119(1), 161–187.
- Koulakov, I., Gordeev, E. I., Dobretsov, N. L., Vernikovskiy, V. A., Senyukov, S., & Jakovlev, A. (2011). Feeding volcanoes of the Kluchevskoy group from the results of local earthquake tomography. *Geophysical Research Letters*, 38, L09305. <https://doi.org/10.1029/2011GL046957>
- Kugaenko, Y., Titkov, N., & Saltykov, V. (2015). Constraints on unrest in the Tolbachik volcanic zone in Kamchatka prior the 2012–13 flank fissure eruption of Plosky Tolbachik volcano from local seismicity and GPS data. *Journal of Volcanology and Geothermal Research*, 307, 38–46.
- Li, K. L., Sadeghisorkhani, H., Sgattoni, G., Gudmundsson, O., & Roberts, R. (2017). Locating tremor using stacked products of correlations. *Geophysical Research Letters*, 44, 3156–3164. <https://doi.org/10.1002/2016GL072272>
- Li, K. L., Sgattoni, G., Sadeghisorkhani, H., Roberts, R., & Gudmundsson, O. (2016). A double-correlation tremor-location method. *Geophysical Supplements to the Monthly Notices of the Royal Astronomical Society*, 208(2), 1231–1236. <https://doi.org/10.1093/gji/ggw453>
- McNutt, S. R. (1992). Volcanic tremor. *Encyclopedia of Earth System Science*, 4, 417–425.
- Métaxian, J.-P., Lesage, P., & Dorel, J. (1997). Permanent tremor of Masaya Volcano, Nicaragua: Wave field analysis and source location. *Journal of Geophysical Research*, 102(B10), 22,529–22,545.
- Métaxian, J.-P., Lesage, P., & Valette, B. (2002). Locating sources of volcanic tremor and emergent events by seismic triangulation: Application to Arenal Volcano, Costa Rica. *Journal of Geophysical Research*, 107(B10), 2243. <https://doi.org/10.1029/2001JB000559>
- Moschella, S., Cannata, A., Di Grazia, G., & Gresta, S. (2018). Insights into lava fountain eruptions at Mt. Etna by improved source location of the volcanic tremor. *Annals of Geophysics*, 61, 4. <https://doi.org/10.4401/ag-7552>
- Nakata, N., Boué, P., Brenguier, F., Roux, P., Ferrazzini, V., & Campillo, M. (2016). Body and surface wave reconstruction from seismic noise correlations between arrays at Piton de la Fournaise Volcano. *Geophysical Research Letters*, 43, 1047–1054. <https://doi.org/10.1002/2015GL066997>
- Ogiso, M., Matsubayashi, H., & Yamamoto, T. (2015). Descent of tremor source locations before the 2014 phreatic eruption of Ontake Volcano, Japan. *Earth, Planets and Space*, 67(1), 206. <https://doi.org/10.1186/s40623-015-0376-y>
- Orchard, J., Ebrahimi, M., & Wong, A. (2008). Efficient nonlocal-means denoising using the SVD. In *2008 15th IEEE International Conference on Image Processing* (pp. 1732–1735). San Diego, CA: IEEE.
- Ozawa, S., Nishimura, T., Suito, H., Kobayashi, T., Tobita, M., & Imakiire, T. (2011). Coseismic and postseismic slip of the 2011 magnitude-9 Tohoku-Oki earthquake. *Nature*, 475(7356), 373.
- Ozerov, A. Y., Firstov, P., & Gavrilov, V. (2007). Periodicities in the dynamics of eruptions of Klyuchevskoi Volcano, Kamchatka, *Volcanism and Subduction: The Kamchatka Region* (pp. 283–291). Washington, DC: American Geophysical Union. <https://doi.org/10.1029/172GM20>

- Patrick, M., Wilson, D., Fee, D., Orr, T., & Swanson, D. (2011). Shallow degassing events as a trigger for very-long-period seismicity at Kilauea Volcano, Hawai'i. *Bulletin of Volcanology*, 73(9), 1179–1186.
- Pitt, A., & Hill, D. (1994). Long-period earthquakes in the Long Valley caldera region, eastern California. *Geophysical Research Letters*, 21(16), 1679–1682. <https://doi.org/10.1029/94GL01371>
- Poli, P., Campillo, M., Pedersen, H., Group, L. W., et al. (2012). Body-wave imaging of Earth's mantle discontinuities from ambient seismic noise. *Science*, 338(6110), 1063–1065.
- Poli, P., Pedersen, H., & Campillo, M. (2012). Emergence of body waves from cross-correlation of short period seismic noise. *Geophysical Journal International*, 188(2), 549–558.
- Ripepe, M., Coltelli, M., Privitera, E., Gresta, S., Moretti, M., & Piccinini, D. (2001). Seismic and infrasonic evidences for an impulsive source of the shallow volcanic tremor at Mt. Etna, Italy. *Geophysical Research Letters*, 28(6), 1071–1074.
- Sens-Schönfelder, C., Snieder, R., & Stähler, S. C. (2015). The lack of equipartitioning in global body wave coda. *Geophysical Research Letters*, 42, 7483–7489. <https://doi.org/10.1002/2015GL065108>
- Senyukov, S. (2013). Monitoring and prediction of volcanic activity in Kamchatka from seismological data: 2000–2010. *Journal of Volcanology and Seismology*, 7(1), 86–97. <https://doi.org/10.1134/S0742046313010077>
- Senyukov, S., Droznina, S. Y., Nuzhdina, I., Garbuzova, V., & Kozhevnikova, T. Y. (2009). Studies in the activity of Klyuchevskoi Volcano by remote sensing techniques between January 1, 2001 and July 31, 2005. *Journal of Volcanology and Seismology*, 3(3), 191–199. <https://doi.org/10.1134/S0742046309030051>
- Seydoux, L., Shapiro, N., de Rosny, J., Brenguier, F., & Landès, M. (2016). Detecting seismic activity with a covariance matrix analysis of data recorded on seismic arrays. *Geophysical Journal International*, 204(3), 1430–1442. <https://doi.org/10.1093/gji/ggv531>
- Seydoux, L., Shapiro, N., de Rosny, J., & Landès, M. (2016). Spatial coherence of the seismic wavefield continuously recorded by the USArray. *Geophysical Research Letters*, 43, 9644–9652. <https://doi.org/10.1002/2016GL070320>
- Shapiro, N. M., Droznin, D. V., Droznina, S. Y., Senyukov, S. L., Gusev, A. A., & Gordeev, E. I. (2017). Deep and shallow long-period volcanic seismicity linked by fluid-pressure transfer. *Nature Geosciences*, 10, 442–445. <https://doi.org/10.1038/NGEO2952>
- Shapiro, N. M., Sens-Schönfelder, C., Lühr, B. G., Weber, M., Abkadyrov, I., Gordeev, E. I., et al. (2017). Understanding Kamchatka's extraordinary volcano cluster. *Eos, Transactions American Geophysical Union*, 98(7), 12–17. <https://doi.org/10.1029/2017EO071351>
- Shaw, H. R., & Chouet, B. (1991). Fractal hierarchies of magma transport in Hawaii and critical self-organization of tremor. *Journal of Geophysical Research*, 96(B6), 10,191–10,207.
- Soubestre, J., Shapiro, N. M., Seydoux, L., de Rosny, J., Droznin, D. V., Droznina, S. Y., et al. (2018). Network-based detection and classification of seismovolcanic tremors: Example from the Klyuchevskoy volcanic group in Kamchatka. *Journal of Geophysical Research: Solid Earth*, 123, 564–582. <https://doi.org/10.1002/2017JB014726>
- Sparks, R., Biggs, J., & Neuberg, J. (2012). Monitoring volcanoes. *Science*, 335(6074), 1310–1311. <https://doi.org/10.1126/science.1219485>
- Stasiuk, M. V., Jaupart, C., & Sparks, R. S. J. (1993). On the variations of flow rate in non-explosive lava eruptions. *Earth and Planetary Science Letters*, 114(4), 505–516.
- Taisne, B., Brenguier, F., Shapiro, N., & Ferrazzini, V. (2011). Imaging the dynamics of magma propagation using radiated seismic intensity. *Geophysical Research Letters*, 38, L04304. <https://doi.org/10.1029/2010GL046068>
- Ukawa, M., & Ohtake, M. (1987). A monochromatic earthquake suggesting deep-seated magmatic activity beneath the Izu-Ooshima Volcano, Japan. *Journal of Geophysical Research*, 92(B12), 12,649–12,663.
- Vidale, J. E. (1986). Complex polarization analysis of particle motion. *Bulletin of the Seismological society of America*, 76(5), 1393–1405.
- Wagner, G. S., & Owens, T. J. (1995). Broadband eigen-analysis for three-component seismic array data. *IEEE Transactions on Signal Processing*, 43(7), 1738–1741.
- Wax, M., & Kailath, T. (1985). Detection of signals by information theoretic criteria. *IEEE Transactions on Acoustics, Speech, and Signal Processing*, 33(2), 387–392.
- White, R. A. (1996). Precursory deep long-period earthquakes at Mount Pinatubo: Spatio-temporal link to a basalt trigger. In *Fire and mud: Eruptions and lahars of Mount Pinatubo, Philippines* (pp. 307–328). Seattle: University of Washington Press. <https://pubs.usgs.gov/pinatubo/white/>
- White, R., Harlow, D., & Chouet, B. (1992). Long-period earthquakes preceding and accompanying the June 1991 Mount Pinatubo eruptions. *Eos, Transactions, American Geophysical Union*, 73, 347.
- Woods, J., Donaldson, C., White, R. S., Caudron, C., Brandsdóttir, B., Hudson, T. S., & Ágústssdóttir, T. (2018). Long-period seismicity reveals magma pathways above a laterally propagating dyke during the 2014–15 Bárðarbunga rifting event, Iceland. *Earth and Planetary Science Letters*, 490, 216–229. <https://doi.org/10.1016/j.epsl.2018.03.020>
- Yukutake, Y., Honda, R., Harada, M., Doke, R., Saito, T., Ueno, T., et al. (2017). Analyzing the continuous volcanic tremors detected during the 2015 phreatic eruption of the Hakone Volcano. *Earth, Planets and Space*, 69(1), 164. <https://doi.org/10.1186/s40623-017-0751-y>